

HOKKAIDO UNIVERSITY

Title	Void fraction distributions of inert gas jets across a single cylinder with non-wetting surface in liquid sodium
Author(s)	Kudoh, Hideyuki; Zhao, Dawei; Sugiyama, Ken-ichiro et al.
Citation	Journal of Nuclear Science and Technology, 49(12), 1175-1185 https://doi.org/10.1080/00223131.2012.739019
Issue Date	2012-11-20
Doc URL	https://hdl.handle.net/2115/53587
Rights	This is an Author's Accepted Manuscript of an article published in Journal of Nuclear Science and Technology, Volume 49, Issue 12, 2012, pages 1175-1185, ©2012 Atomic Energy Society of Japan, available online at: http://www.tandfonline.com/10.1080/00223131.2012.739019.
Type	journal article
File Information	JNST49-12_1175-1185.pdf



Hokkaido University Collection of Scholarly and Academic Papers : HUSCAP

ARTICLE

Void Fraction Distributions of Inert Gas Jets across a Single Cylinder with Non-Wetting Surface in Liquid Sodium

Hideyuki KUDOH[a,*],Dawei ZHAO[a], Ken-ichiro SUGIYAMA[a],

Tadashi NARABAYASHI[a], Hiroyuki OHSHIMA[b] and Akikazu KURIHARA[b]

[a]*Hokkaido University, North 13 West 8, Kita-ku, Sapporo 060-8628, Japan;* [b]*Japan Atomic Energy Agency, Narita, O-arai-machi, Ibaraki311-1393, Japan*

(Received)

Little work on the void fraction behaviors along structural materials with poor-wettability for liquid metals has been performed. In the present study, void fraction behaviors around a single cylinder with non-wetting surface condition were quantitatively discussed by using a gas jet-cylinder system where the impinging jet flow, the boundary layer flow, the separation flow, and the wake flow appear.

One cylinder with a non-wetting surface and two cylinders with a wetting surface were used to vary the wettability for liquid sodium, and void fraction distributions were measured around the cylinders. In the case of wetting condition, void fraction distributions around the cylinder decrease clearly in the backward region of the cylinder, and liquid-rich region is formed due to bubble separation from the cylinder surface. On the other hand, under non-wetting condition, because of two-phase flow without bubble separation on the cylinder surface, void fraction distributions show almost steady values around the cylinder compared

[*]Corresponding author. E-mail: k.hide.16@eng.hokudai.ac.jp

to those with wetting surface. The void behaviors on a non-wetting surface were also confirmed by a visualization experiment conducted in water. The observed differences can be basically attributed to the work of adhesion required for liquid-solid interfacial separation.

KEYWORDS: wetting, non-wetting, two-phase flow, void fraction, liquid sodium, single cylinder, gas jet

1. Introduction

Numerous studies on gas-liquid two-phase flow for many geometric configurations used in the energy industries have been carried out by using water as liquid phase, which makes wetting of structural materials at ordinary temperatures. Because of the experimental difficulty in liquid metal systems, the results of these studies apply to them based on the similarity. The results by Joo and Dhir, and Inoue *et al.* focusing on a bubbly cross flow around a circular cylinder are therefore compared to the present results at wetting surface condition as shown later [1], [2].

However, for complex systems the similarity is not assured, experiments using liquid metals are required. Studies by Mishima *et al.* and Saito *et al.* on visualization and void fraction measurement of gas-liquid metal two-phase flow performed by using neutron radiography and image processing techniques are typical examples [3], [4]. The exact similarity between liquid metals and water is also not assured under the condition of non-wetting liquid metal systems.

It is reported that the gas-water two-phase flow in a non-wetting tube is significantly different from that in a wetting tube. Takamasa *et al.* observed in an upward gas-liquid two-phase flow that the water flows in the center core in a non-wetting tube, whereas the water flows in the vicinity of the tube wall in a wetting tube [5]. This is a typical example. Although the different behavior of gas-liquid metal two-phase flow between wetting condition and non-wetting condition has been pointed out, little work quantitatively clarified has been performed. In particular, liquid sodium, which is employed as a coolant of fast breeder reactors, is known that the wettability varies depending on temperature and structural materials [6], [7]. Basic understanding for the difference in two-phase flow between wetting and non-wetting conditions is primarily important from the viewpoint of thermal hydraulic design and safety evaluation in both normal and accidental conditions.

In the present study focusing on inert gas-liquid sodium two-phase flow, the difference in void fraction behaviors around a single cylinder between non-wetting and wetting condition is examined. A gas jet-cylinder system, which consists of the impinging jet flow and the boundary layer flow in the forward region, and the separation flow and the wake flow in the backward region, is selected for quantitative examination on the difference in both conditions. By using the single system, the characteristics in each flow field as well as the relationship between flow fields, which have not been quantitatively discussed so far, are obtained. The local void fraction around a single cylinder with wetting condition or non-wetting condition was measured by using resistivity probes.

2. Experiment

2.1. Experimental apparatus

Figure 1 shows a schematic diagram of experimental apparatus. The apparatus consisted of a test vessel, a sodium storage tank, a sodium mist trap, and an argon gas heater. All sections were made of stainless steel, of which surfaces were covered with thermal insulators after assuring air tightness and installing sheathed heaters. The test vessel was 1000 mm high with 80 mm in inner diameter. Circulation pipes were installed on the test vessel to reduce temperature gradient in the vertical direction. Sodium in the storage tank could be heated up to a desired temperature by using the sheathed heaters. After a few times gas displacement in the test vessel with high-purity argon gas, sodium was charged from the storage tank to the test vessel by high-purity argon gas pressure and the liquid level in the test vessel was adjusted to 700 mm in height. The sodium temperature in the storage tank was kept to be 110°C during the charging process, so that oxygen solubility in the test vessel was expected to be less than 10 ppm during measurement. The argon gas heated up to a desired temperature by the gas heater section was injected in the upward direction into the stationary

liquid sodium from a gas nozzle located below a test cylinder. The mist trap was installed to catch sodium vapor and/or sodium mist which were included in the exhaust.

Figure 2 shows a schematic of the test section. A test cylinder was inserted horizontally into the test vessel. The outer diameter of the cylinder was 20 mm. The nozzle consisted of a head and a pipe made of stainless steel, and the nozzle hole diameter, d , was 3.5 mm. The distance from the nozzle exit to the forward stagnation point of the cylinder was 25 mm. Void fraction distributions were measured with four void probes set parallel to the test cylinder as shown in Figure 2. It consists of a stainless-steel wire (0.5 mm O.D.) and two silicone rubber tubes (1 mm O.D. and 0.5 mm I.D.). The stainless steel wire is insulated electrically with the silicone rubber tubes except the detection part of 1 mm long. The four void probes were placed using ring-shaped spacers at the distances from the cylinder surface, δ = 1, 2, 3, and 4 mm, respectively. Every detection part was set in the plane with the cylinder cross section through the jet axis. Two spacers were mounted on the cylinder with 80 mm distance from each other; corresponding to the inner diameter of the cylindrical vessel. In order to keep the probe positions against high speed gas jets, the probes were strained through the spacers. The test cylinder was designed to be capable of rotating around its axis together with the four void probes. This means the void fractions could be measured at any azimuthal angle, θ, as shown in Figure 2. Thus the circumferential distributions of local void fraction in the plane with the cylinder cross section through the gas jet axis could be obtained by rotating them in 360 degrees. In addition to these probes, as shown in Figure 2, an I-shaped probe movable in the vertical direction through the jet axis of the nozzle was also set.

The circuit for local void fraction measurement consisted of an AC power source, a discriminator, and a data logger. The AC of 3 V in 10 kHz was supplied between the test cylinder and the probe detection part. When the probe detection part is in contact with gas, a

high voltage, almost corresponding to the source voltage, is output. When it is in contact with water including small amount of sodium chloride or liquid sodium, output voltages were almost zero. The threshold value to distinguish gas and liquid was set at 80% of the input voltage for both water and sodium experiments. Both signals of gas and liquid were automatically distinguished by the discriminator and recorded by the data logger. After the influence of the measuring time on local void fraction due to a long-period circulation of the flow field was examined, the signals were obtained at a total measurement time of 5 seconds. Local void fraction, α, was determined as the ratio of summation of bubble dwell time, t_i (time required for a bubble to pass the detection part of a void probe), to total measurement time, t_{total}:

$$\alpha = \sum t_i / t_{total} . \quad (1)$$

The accuracy of the present system for void fraction measurement was checked by a preliminary experiment conducted in a water pool. In the preliminary measurement using the I-shaped probe movable in the both vertical and radial directions, the vertical and radial void fraction distributions of upward gas-free-jet, without the test cylinder, were checked to be a good agreement with an empirical correlation proposed by Castillejos and Brimacom using a stainless steel detection part of 0.3 mm in diameter within ± 15% [8].

Because of the non-wettability of the probe detection part in liquid sodium, as described later, the response for phase change at the probe detection part in liquid sodium are faster than that in water. Thus the void fraction measurements in liquid sodium are considered to be more accurate. In addition to that, the effect of the shape of the wire probes on the flow field was examined by comparing the void fraction values measured by the wire probes and the I-shaped probe vertically inserted from the top of the test vessel as shown in Figure 2. These values were measured at δ = 1, 2, 3, and 4 mm respectively in the backward stagnation point of the test cylinder (θ = 180°) in liquid sodium. The results from these probes show a good

agreement within ± 15 %.

The gas jet velocities at the nozzle exit, u, were obtained by dividing gas flow rates, V, by the cross-sectional area of the nozzle:

$$u = \frac{V}{\pi d^2/4}. \tag{2}$$

The experimental conditions are summarized in **Table 1**. The sodium temperature was always kept at 200°C for assuring the reliability as electrical insulator of silicone rubber tubes used in the present resistivity probes. Because large generation of sodium mist and sodium vapor was expected under high gas jet velocity conditions, the maximum gas jet velocity in liquid sodium was limited to be lower than that in water.

In this study, we employed a gas jet-cylinder system. Although void fraction distributions around a cylinder in bubbly flow have been investigated by a few workers, no data has been obtained in the gas jet- cylinder systems even in water. Thus the void fraction distributions were firstly measured in water to investigate the dependency of void fraction distributions on the experimental geometry. Then the measurements were conducted in liquid sodium with different wettability. In the case of water experiments, a small amount of sodium chloride was added into water in order to keep the electrical conductivity.

2.2. Test cylinders with wetting and non-wetting surface

Liquid sodium has a property that its contact angle, θ_c, changes with the wall materials and temperature. For example, a sodium droplet in low temperature at iron and nickel surfaces shows non-wetting property, $\theta_c > 90°$, as shown in **Figure 3**(a), due to the existence of a thin oxide film. However, when the sodium temperature increases, complete reduction of the oxide film due to the chemical reactions takes place and the clean metal surface is well wetted by liquid sodium. According to the study of Addison *et al.* using the vertical plate

method, the contact angle sharply changes to zero within a few degrees of "the critical wetting temperature" [6]. The critical wetting temperatures for iron and nickel were reported to be 140°C and 195°C, respectively. The behavior of austenitic stainless steels is different from iron and nickel. Hodkin *et al.* observed in their work with the sessile drop method that sodium droplet at stainless steel surfaces shows a non-wetting property of θ_c = 140° below 280°C and above 280°C the contact angle gradually decreases and reaches to a value of 20° above 550°C, as qualitatively shown in Figure 3(a) [7].

In our preliminary experiment, it was confirmed that gas phase signals from the resistivity void probe using stainless steel wire suddenly disappear at around 300 °C. This means that the detection part of the void prove is steady covered (wetted) with sodium. In addition to this, the reliability as electrical insulator of silicone rubber tubes used in the present resistivity probes is assured up to 200°C. Above the temperature, because of the degradation of silicone rubber tube, its performance for electrical insulator and non-wettability against sodium would not be expected. Based on these results, our resistivity probes were used at 200°C non-wettable for sodium.

For the experiment under non-wetting condition, stainless steel was chosen for cylinder material because its non-wettability against sodium is assured at 200°C. For wetting condition, a nickel-plated stainless steel cylinder was prepared. The sodium temperature was adjusted at 200°C, which is greater than the critical wetting temperature of nickel, so that the surface is wetted by liquid sodium.

We employed another test cylinder with an iron oxide film, on which surface wetting against sodium is expected. According to Montemor *et al.*, an external iron oxide region is produced on the surface of austenitic stainless steels during two-hour heating at temperatures between 250°C and 450°C in air [9]. The thickness of an external iron oxide region is around 20 nm and thus the nickel and chromium rich region exists inside the iron oxide region.

Based on their study, the stainless steel cylinder with an iron oxide film, which was heated at 300°C for 4 hours in the atmosphere, was prepared as a wetting cylinder. The sodium temperature during the experiment was again adjusted at 200°C, which is greater than the critical wetting temperature of iron, 140°C. Thus it is expected that the oxygen in the iron oxide region is easily reduced due to formation of Na_2O and the resulted iron-rich surface is wetted by liquid sodium with a very low θ_c.

The wettability of cylinder surface against liquid sodium was confirmed after each experiment. **Figure 4** compares the appearances of sodium droplets on the stainless steel cylinder and the iron-rich surface cylinder after draining process of liquid sodium. These pictures were taken in the atmosphere after the temperature of the experimental apparatus was cooled down to the room temperature. Because of the irreversibility of wettability, it is reasonable to consider that the contact angles of liquid droplets were maintained during the cooling process [10]. For the stainless steel cylinder, spherical-shaped droplets were observed and $\theta_c \approx 125°$ was measured from the picture. Although the measured contact angle was somewhat lower than the result obtained by Hodkin *et al.*, non-wetting of stainless steel against liquid sodium was confirmed. On the other hand, for the iron-rich surface cylinder, flat shaped droplets with $\theta_c \approx 20°$ were observed. This proves an excellent wetting of the iron-rich surface with liquid sodium during the experiment.

3. Results and discussion

3.1. Void fraction distribution in water

As mentioned above, the gas jet-cylinder system was employed in this study. However, even in water, there have been no previous studies which measured void fraction distributions around a cylinder with gas jet impingement. Thus it is needed to investigate the differences of flow characteristics between the present system and bubbly flow-cylinder system which

has been studied by Joo and Dhir, and Inoue *et al.* [1], [2]. For that reason, void fraction distributions around a cylinder were measured in water-argon gas system by using the test section shown in Figures 1 and 2. The contact angle between the cylinder surface of stainless steel without surface treatment and water was confirmed by direct reading from the pictures of water droplets and it was 30°. Therefore, a typical result under wetting condition was obtained.

Figure 5 shows circumferential void-fraction distributions around a single cylinder in water for different gas jet velocities. The gas jet velocities were 93, 186, and 372 m/s, respectively. Since the measured results are almost symmetrical about the center line of the gas jet, the averaged values in the range from θ = 0° to 180° are shown in the figure. In all cases shown here, the void fractions are highest at θ = 0° and lowest at θ = 180°. In the forward region of the cylinder (0° < θ < 90°), void fractions keep relatively higher value and then steeply decreases toward θ = 180°. For higher gas jet velocities, u = 186 and 372 m/s, the void fractions at the forward stagnation point of the cylinder (θ = 0°) show unity without depending on the distance from the cylinder surface. The region from the gas nozzle exit to the forward stagnation point of the cylinder is considered to be filled with gas phase because a large volume of gas is injected from the nozzle under the high gas jet velocity conditions. However, for the lower gas jet velocity of u = 93 m/s, void fractions at θ = 0° are not reached α = 1 due to a small amount of water entrained into the gas jet.

Focusing on the cylinder backward region (90° < θ < 180°), void fractions steeply decrease toward the backward stagnation point of the cylinder. When focusing on the distance from the cylinder surface, the decrease of void fraction in the backward of the cylinder begins from the vicinity of the surface and void fractions at some distance from the cylinder surface is higher than those near the surface. Therefore the rapid decrease in void fractions can be attributed to the bubble separation from the cylinder surface and the presence

of liquid-rich region was confirmed in the backward of the cylinder.

Joo and Dhir measured void fraction distributions around a cylinder horizontally set in a bubbly flow with a free stream void fraction of 0.25 [1]. For their low velocity results, the void fractions near the forward region showed values higher than the free stream void fraction due to the stagnant behavior of bubbles in the region, while the void fractions in the backward region showed values lower than the free stream void fraction due to the separation of bubbly flow from the cylinder surface. In the present system, the impingement of the gas jet makes the highest void fraction for the forward stagnation point. For their high velocity results, the void fraction value measured at δ = 4 mm of the forward stagnation point showed the lowest value lower than the value of the backward stagnation point, which would be attributed to the stagnant behavior of water trapped in the region. The interesting fact observed by them was not observed in the present results because the inertial force of gas jet with high velocities prevents the accumulation of water in the forward stagnation point.

Inoue *et al.*also studied the wake region of uniform bubbly flows across a cylinder and reported the existence of liquid-rich region behind the cylinder [2]. They suggested that the liquid-rich region is formed by the balance between buoyancy force of bubbles and the reverse flow in the wake. The same type of balance also causes the liquid-rich region in the gas jet-cylinder system selected in the present study. Therefore, the existence of the liquid-rich region near the backward region irrespective of geometrical difference between the gas jet-cylinder system and the uniform bubbly flow-cylinder one can be considered a common behavior of water-gas flow across a cylinder with wetting surface.

3.2. Void fraction distribution in liquid sodium

Figure 6 shows void fraction distributions around a stainless steel cylinder in liquid sodium. As mentioned above, the test cylinder and the nozzle made of stainless steel was

non-wetting because of the measurement at low temperature liquid sodium. The gas jet velocities were 90, 150, and 300 m/s, respectively. For only u = 90 m/s, the probe of δ = 3 mm failed to obtain void fraction at θ = 180° due to a large disturbance for the signals. Compared to the results in water with the wetting cylinder, void fractions around the non-wetting cylinder show a limited variation from 0.5 to 0.9. In addition, void fraction distributions show a weak dependency on the gas jet velocity under the present experimental condition.

The most obvious differences of void fraction distributions between water and liquid sodium are seen at θ = 0° and 180°. Void fraction at θ = 0° shows $0.6 < \alpha < 0.8$ even at the highest gas jet velocity (u = 300 m/s). The void fractions at θ = 180° also remain $0.5 < \alpha < 0.8$ in all cases. Therefore the void fractions under the non-wetting condition do not show a rapid decrease toward θ = 180° as seen in water. It is easily supposed that the gas jet flowing along the cylinder circumference from the forward stagnation point to the backward one without separation results in a narrow variation in void fractions around the non-wetting cylinder. Focusing on the distance from the cylinder surface, void fractions at δ = 1 mm are higher than those at δ = 4 mm in most angles. This result indicates that bubbles mainly flow near the surface along the cylinder. Therefore the higher void fraction at the backward region of the cylinder can be attributed to the no bubble separation from the surface.

Figure 7 shows the void fraction distributions around the iron-rich surface cylinder and the nickel-plated cylinder in liquid sodium under wetting condition, the nozzle was also wetted. The gas jet velocities were 30, 90, and 150 m/s, respectively. The measuring points of void fraction in the iron-rich surface cylinder and the nickel plated cylinder were reduced to δ = 2 and 4 mm, and δ = 4 mm, respectively. It is obvious for all cases of 30, 90, and 150 m/s that the void fraction distributions measured at δ = 4 mm in the nickel-plated cylinder are a fairly good agreement with those measured at δ = 4 mm in the iron-rich surface

cylinder. It is therefore reasonable to regard that the void fraction data obtained in the two cylinders have a fairly good accuracy for discussing the difference in void fraction distributions between wetting and non-wetting conditions.

In comparison of Figure 7 with Figure 6 for void fraction distributions at 90 and 150 m/s, a difference between the wetting condition and the non-wetting conditionis clearly observed in the backward region. The void fractions under wetting condition decrease from θ = 120° and reach to values of α < 0.3 at θ = 180° as show in Figure 7, while the void fractions at δ = 2 and 4 mm under non-wetting condition are almost constant values of 0.55 to 0.65 in the same region as shown in Figure 6. It is also obvious in Figure 7 under wetting condition that the highest void fraction always appears in the forward stagnation point. The characteristic in the forward stagnation point is not observed in Figure 6 under non-wetting condition. The behavior of void fraction distributions in the three cases of u = 30, 90, 150 m/s shown in Figure 7 is therefore reasonable to be qualitatively similar to those of u = 93 m/s in water shown in Figure 5, except for the inverse relationship for values at δ = 2 and 4 mm in the backward region between Figure 7 and Figure 5.

Figures 8 and 9 compare the void fraction distributions of water and sodium under wetting condition with those of sodium under non-wetting condition at δ = 2 and 4 mm, respectively, from the viewpoint of Reynolds number and Weber number based on the nozzle exit condition. The Reynolds number and the Weber number of gas jet at the nozzle exit in water at u = 19 and 56 m/s are 1.4 times and 1.1 times as large as those in sodium at u = 30 and 90 m/s, respectively. This means the inertial force of gas jet in water at u = 19 and 56 m/s is larger than that in sodium at u = 30 and 90 m/s, respectively. From this physical aspect, it is qualitatively reasonable in Figures 8 and 9 that the void fraction distributions in water at u = 19 and 56 m/s always show values larger than those in liquid sodium under wetting condition at u = 30 and 90 m/s in the forward region of 0° < θ < 90° except for somewhat

small values of water at δ = 2 mm in u = 19 m/s.

Differences of void fraction distributions between sodium under wetting condition and water at δ = 2 and 4 mm in the backward region of 120° < θ < 180° would mainly originate in the different behavior between bubbles in sodium and those in water in the process of the separation of two-phase jet flow decelerating along the cylinder surface because the surface tension of sodium is around 3 times as large as that of water. This different behavior should be examined in the future study. It is also mentioned that the difference in sodium data between wetting and non-wetting conditions near the forward stagnation point would originate in the difference of gas jet behavior between the wetting nozzle and the non-wetting nozzle, and the difference of stagnant behavior of bubbles between wetting surface and non-wetting surface. This point is again considered in Section 3.3.

3.3. Visualization with water

In this section, the interaction between bubbles and solid surfaces under wetting and non-wetting conditions, which governs the separation behavior in sodium and water, is again discussed, based on the visualization experiment at u = 19 m/s using water shown in Figures 10 and 11. The experimental geometry is the same as that shown in Figure 2, except for using a rectangular aquarium made of acrylic. Visualized images of gas-liquid two-phase flow were taken by a high-speed camera at a frame speed of 2000 fps.

In this experiment, a new wetting cylinder was made of acrylic and exposed to plasma (provided by NISSIN Inc.) to produce low contact angle. A non-wetting cylinder was made of polycarbonate and a water-repellent coating (provided by Ascot Corp.) was applied to the surface to produce high contact angle. According to these suppliers, the contact angles against water on the wetting and non-wetting surfaces are approximately 10° and 150°, respectively, which are near those in the sodium experiments shown in Figure 4. The details

of the mechanisms to control contact angles are described, for example, in Reference [11]. Two types of gas nozzles were also employed. In the case of wetting condition, stainless steel nozzle was used and the contact angle was confirmed to be approximately 30°. In the case of non-wetting condition, stainless steel nozzle coated with the water-repellent material was used and the contact angle was approximately 150°. The coating was conducted on the end, side, and inner surfaces of the nozzle. The soundness of coating for the cylinder and the nozzle was confirmed before and after each run by reading the contact angles from pictures of water droplets remaining on the surfaces.

3.3.1 Wetting condition

Figure 10 shows visualized images of gas jet behavior around the wetting cylinder at u = 19 m/s. A typical bubble just before being detached from the wetting nozzle is vertically elongated to the forward stagnation point of the cylinder (0 ms). The bubble is divided by the cylinder in the horizontal direction (40 ms) and rises along the cylinder circumference (60 ms). The bubble flow is then bended into the tangential direction at θ = 120° without rising straight up from the cylinder surface of θ = 90° (80 ms). This behavior may attribute to the Coanda effect; the tendency of fluid to flow along a curved surface. In other words, the gas jet under the present experimental condition may have a property of so called "wall jet."

In the backward region of the cylinder, bubbles are separated from the cylinder surface at the vicinity of θ = 120° (100 ms). Then the separated bubbles are directed toward the center line. As a result a triangle shaped liquid-rich region is formed near the backward stagnation point (100 ms). The separation behavior of bubbles is well correspondent to a steep gradient from θ = 120° and 140° for the void fraction distribution of δ = 2 and 4 mm, respectively, at u = 19 m/s shown in Figures 8 and 9. A bubble just after being detached from the wetting nozzle gets into touch with the forward region of the cylinder again (120 and 140 ms). The behavior is correspondent to that between 0 and 40 ms.

3.3.2 Non-wetting condition

Figure 11 shows visualized images of gas jet behavior around the non-wetting cylinder at u = 19 m/s. A typical bubble just before being detached from the non-wetting nozzle gets into touch with the forward stagnation point of the cylinder (0 ms). The forefront of bubble smoothly enters the backward region (40ms) and reaches to the region near the backward stagnation point with a sliding-motion along the cylinder circumference (60 ms). Compared to the bubble behavior until this time period, it is obvious that the bubble at 40 ms and 60 ms in Figure 10 shows a stagnant behavior because of wetting surface cylinder. The bubbles cover the backward region without the separation as shown at 80 ms and then move to wake region with an adhesive behavior to the backward surface (100 and 120 ms). In addition, it should be also mentioned from the adhesive behavior that a small part of the large bubbles, which already passed through the cylinder, remains on the surface near θ = 180° (40 ms and 140 ms).

The different behavior between wetting and non-wetting surfaces in water shown in Figures 10 and 11 can be understood by considering the physics for the adhesion of water on these surfaces. As shown in Figure 3, a water droplet on a wetting surface spreads with a small contact angle whereas a gas bubble on a non-wetting surface spreads with a large contact angle. The work of adhesion, W, is defined as the necessary work required for making a liquid-solid interface separation and expressed by following Young-Dupré's equation:

$$W = \sigma(1+\cos\theta_c), \tag{3}$$

where σ is surface tension [12]. The work of adhesion on wetting surface (θ_c < 90°) is larger than that on non-wetting surface (θ_c > 90°). Therefore, under wetting condition, a bubble in liquid is difficult to produce a new gas-solid interface because the work of adhesion is larger than the surface tension for making the bubble. On the other hand, when a bubble contacts a

solid surface under non-wetting condition (θ_c > 90°), making a gas-solid interface is more energetically stable rather than making a gas-liquid interface (a bubble).

Because of the small work of adhesion, gas bubbles under non-wetting condition tend to stay on the surface and show a sliding-motion along the cylinder circumference. This is the reason that a two-phase jet flow field without separation from the cylinder surface, similar to the well-known inviscid flow around a cylinder, is observed in Figure 11. Based on this consideration, it is reasonable that the gas jet-sodium two-phase flow across a cylinder under non-wetting condition causes the monotonous void fraction distributions without decreasing in the backward region as shown in Figure 6.

3.3.3 Effects of nozzle wettability

The effects of nozzle surface wettability on the void fraction distributions should be taken into account. Sano and Mori suggested from their experiments in both nitrogen-mercury and oxygen-molten silver systems, which were intended for a bottom-blown converter in steel making process, that the outer diameter of the nozzle should be the characteristic length for a single bubble growth behavior because the bubble entirely spreads over nozzle surface due to the non-wettability of liquid metals [13]. However, the range of application of their suggestion is limited in the single bubble regime where the bubble formation at the nozzle exit is governed by a static balance of surface tension and buoyancy force acting on a bubble.

The same kind of behavior was also confirmed in Figure 11 conducted by using the non-wetting nozzle. Bubbly jet discharged at a low velocity of 19 m/s in the range of the bubbling regime shows sliding-motion along the nozzle end surface and side surface, and occasionally spread to the lower side of the nozzle as shown at 20, 40 and 120 ms in Figure 11. Related to this unstable motion at the nozzle exit, the bubble behavior between the nozzle exit and the forward stagnation point of cylinder is also unstable compared to that in Figure 10 conducted by using the wetting nozzle. Therefore the profile lines of bubbles shown in the

right-hand side at each time step of Figure 11 get clearly distorted compared to those in Figure 10. In addition, four large bubbles numbered impinge to the cylinder in Figure 11 while three large bubbles numbered impinge to the cylinder in Figure 10. The increase for number of large bubbles produced during the same time period would also originate in the instability of gas jet on the non-wetting nozzle.

This behavior also suggests an easy water entrainment into the gas jet injected from non-wetting nozzle. The water entrainment into bubbly jet flows is basically caused through the bottom side of bubbles downstream due to the relative velocity between the bubbles downstream decelerated and the bubbles upstream injected with a high velocity from the nozzle. The main water-entrainment in the bubbling regime is basically same in high gas-jet velocity. Therefore there is a possibility that the low void fractions, corresponding to a high sodium entrainment into the gas jet, near the forward stagnation point observed in Figures 8 and 9 for sodium under non-wetting condition, as well as the low values there in Figure 6, originate in the same kind of instability on a non-wetting stainless steel nozzle. Based on this consideration, void fraction distributions higher than those in Figure 6 are expected in the experiment with non-wetting cylinder and wetting nozzle for sodium. An experiment to separate the effect of nozzle should be conducted in the future study.

4. Conclusions

The void fraction behaviors of gas-sodium two-phase flow across the non-wetting and wetting cylinders were experimentally investigated by using gas jet-cylinder systems, which are capable of investigating the characteristics of both the gas jet itself and the flow fields around the cylinder with different surface condition. The following conclusions were obtained:

1. Void fraction distributions around a non-wetting cylinder in liquid sodium show a very

narrow variation from the forward stagnation point to the backward one without showing bubble separation in the backward region. On the other hand, void fraction distributions around a wetting cylinder in water shows a steep decrease in the backward region due to bubble separation.

2. Void fraction distributions around wetting cylinders in liquid sodium are qualitatively similar to those around a wetting cylinder in water. However the decrease of void fraction distributions in liquid sodium is milder than that in water in the backward region.
3. The visualization experiments demonstrated that the difference in void fraction distributions between non-wetting surface and wetting surface is mainly attributed to the difference in the work of adhesion between them. This means that viscous behavior with separation in two-phase jet flow appears on wetting surface whereas inviscid flow-like behavior without separation in two-phase jet flow appears on non-wetting surface.
4. The difference of void fraction distributions between sodium under non-wetting condition and water and sodium under wetting condition near the forward stagnation point where the gas jet impinges is qualitatively understood by the entrainment of sodium into the gas jet originating in the instability on non-wetting nozzle. The non-wetting and wetting effects of nozzle should be further discussed in the future paper.

Nomenclature

d : nozzle diameter [mm]

t_i : dwell time of i-th bubble [ms]

t_{total} : total measurement time [ms]

u : gas jet velocity at nozzle exit [m/s]

V : volume flow rate of gas injection [m^3/s]

W : work of adhesion [N/m]

Greek Letters

α : time averaged local void fraction [-]

δ : distance between probe and cylinder surface [mm]

θ : peripheral angle from the forward stagnation point of cylinder [degrees]

θ_c : contact angle [degrees]

σ : surface tension [N/m]

References

[1] Y. Joo, V.K. Dhir, An experimental study of drag on a single tube and on a tube in an array under two-phase cross flow, *Int. J. Multiphase Flow*, 20[6], (1994), pp. 1009-1019.

[2] A. Inoue, Y. Kozawa, M. Yokosawa, S. Aoki, Studies on two-phase cross flow. Part I: Flow characteristics around a cylinder, *Int. J. Multiphase Flow*, 12[2], (1986), pp. 149-167.

[3] K. Mishima, T. Hibiki, Y. Saito, H. Nishihara, Y. Tobita, K. Konishi, M. Matsubayashi, Visualization and measurement of gas-liquid metal two-phase flow with large density difference using thermal neutrons as microscopic probes, *Nucl. Instrum. Methods Phys. Res. A*, 424, (1999),pp. 229-234.

[4] Y. Saito, K. Mishima, Y. Tobita, T. Suzuki, M. Matsubayashi, Measurements of liquid-metal two-phase flow by using neutron radiography and electrical conductivity probe, *Exp. Therm. Fluid Sci.*, 29, (2005), pp. 323-330.

[5] T. Takamasa, T. Hazuku, T. Hibiki, Experimental study of gas-liquid two-phase flow affected by wall surface wettability, *Int. J. Heat Fluid Flow,* 29, (2008), pp. 1593-1602.

[6] C.C. Addison, *The chemistry of the liquid alkalimetals*, John Wiley & Sons, New York, (1984), pp. 248-268, ISBN0471905089.

[7] E.N. Hodkin, D.A. Mortimer, M. Nicholas, The wetting of some ferrous materials by sodium, *Proc. Int. Conf. Liquid Alkali Metals*, Nottingham, England, April 4-6, 1973, (1973), pp. 167-170, ISBN 0901948772.

[8] A.H. Castillejos, J.K. Brimacombe, Measurement of physical characteristics of bubbles in gas-liquid plumes: Part II. Local properties of turbulent air-water plumes in vertically injected jets, *Metall. Trans. B*, 18B, (1987), pp. 659-671.

[9] M.F. Montemor, A.M.P. Simoes, M.G.S. Ferreira, M.Da Cunha Belo, The role of Mo in

the chemical composition and semiconductivebehavior of oxide films formed on stainless steel, *Corrosion Science*, 41, (1999), pp. 17-34.

[10] B. Longson, J. Prescott, Some experiment on the wetting of stainless steel, nickel and iron in liquid sodium, *Proc. Int. Conf. Liquid Alkali Metals*, Nottingham, England, April 4-6, 1973, (1973), pp. 171-176, ISBN 0901948772.

[11] T. Ishii, M. Koishi, T. Tsunoda, *Wettability Technology Hand book* [in Japanese], Techno-system, Tokyo, (2001), pp. 3-34, ISBN4924728381.

[12] A.W. Adamson, A.P. Gast, *Physical Chemistry of Surface, 6th Ed.*, Wiley-Interscience, New York, (1997), pp. 347-389, ISBN0471148733.

[13] M. Sano, K. Mori, Bubble formation from single nozzles in liquid metals, *Trans. JIM*, 17, (1976), pp. 344-352.

Table

Table 1 Experimental conditions in void fraction measurements

	Wetting		**Non-wetting**
	Water	Sodium	Sodium
Test cylinder	Stainless steel	Iron-rich surface Nickel coating	Stainless steel
Temperature [ºC]	20	200	200
Gas jet velocity, u [m/s]	19 - 372	30 - 150	30 - 300
Contact angle, θ_c [º]	30	20	125

Figure captions

Figure 1 Schematic of experimental apparatus

Figure 2 Schematic of test cylinder and void probes

Figure 3 Contact angles of droplets and bubbles on wetting and non-wetting surfaces

Figure 4 Solid droplets on cylinder surface taken after experiments

Figure 5 Void fraction distributions around a wetting cylinder in water

Figure 6 Void fraction distributions around a non-wetting cylinder in liquid sodium

Figure 7 Void fraction distributions around a wetting cylinder in liquid sodium

Figure 8 Comparison of void fraction distributions (δ = 2 mm)

Figure 9 Comparison of void fraction distributions (δ = 4 mm)

Figure 10 Visualized images of a gas jet around a wetting cylinder (u = 19 m/s)

Figure 11 Visualized images of a gas jet around a non-wetting cylinder (u = 19 m/s)

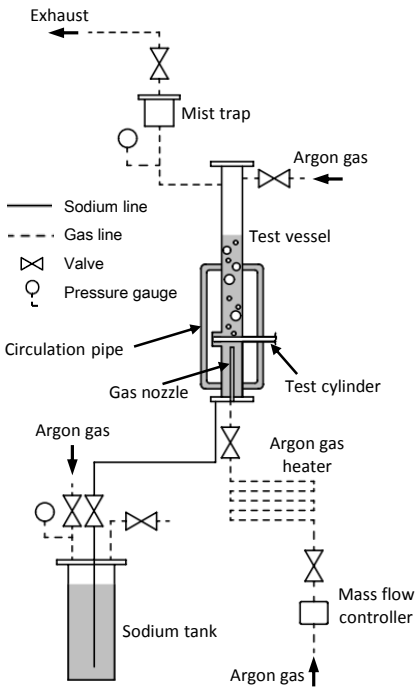


Figure 1 Schematic of experimental apparatus

H. Kudoh:

Void Fraction Distributions of Inert Gas Jets across a Single Cylinder with Non-Wetting Surface in Liquid Sodium

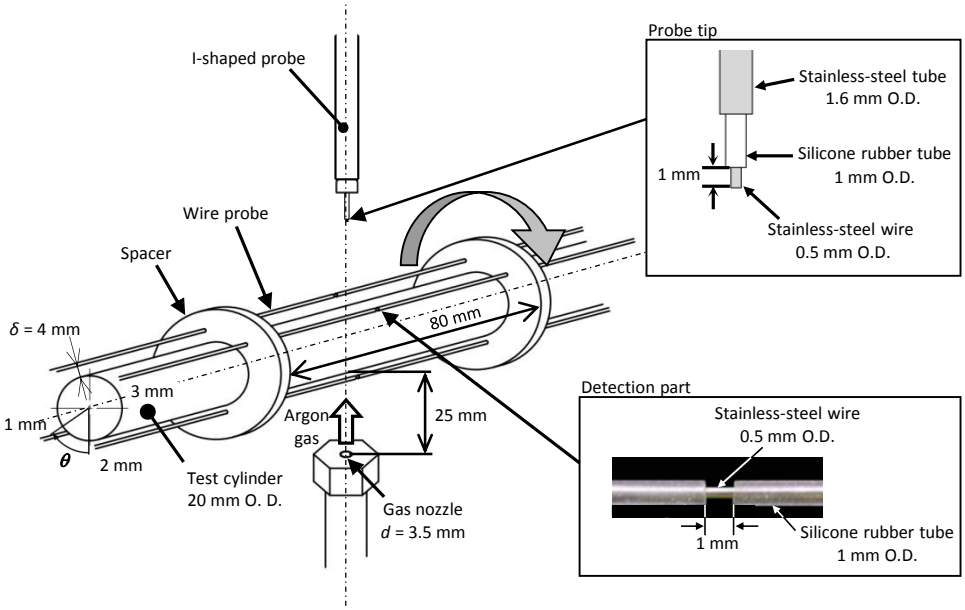


Figure 2 Schematic of test cylinder and void probes

H. Kudoh:

Void Fraction Distributions of Inert Gas Jets across a Single Cylinder with Non-Wetting Surface in Liquid Sodium

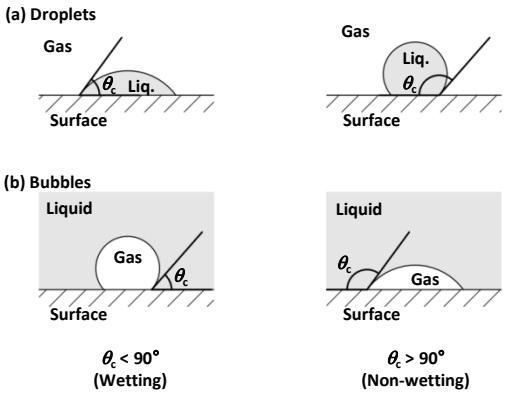


Figure 3 Contact angles of droplets and bubbles on wetting and non-wetting surfaces

H. Kudoh:

Void Fraction Distributions of Inert Gas Jets across a Single Cylinder with Non-Wetting Surface in Liquid Sodium

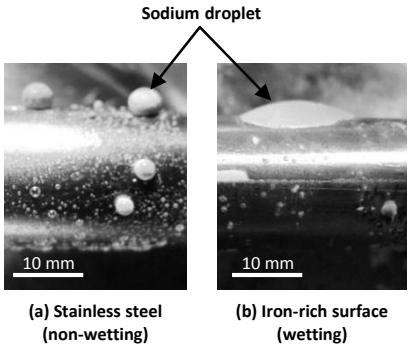


Figure 4 Solid droplets on cylinder surface taken after experiments

H. Kudoh:

Void Fraction Distributions of Inert Gas Jets across a Single Cylinder with Non-Wetting Surface in Liquid Sodium

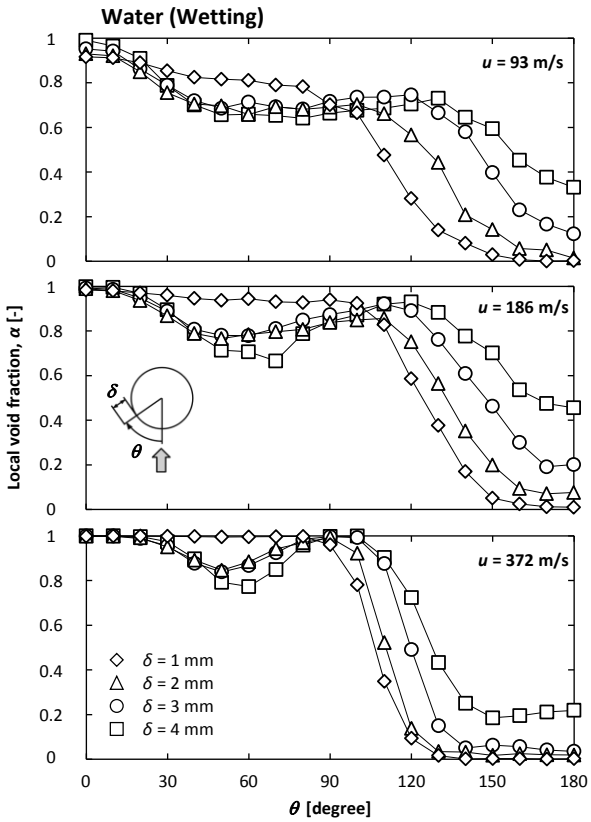


Figure 5 Void fraction distributions around a wetting cylinder in water

H. Kudoh:

Void Fraction Distributions of Inert Gas Jets across a Single Cylinder with Non-Wetting Surface in Liquid Sodium

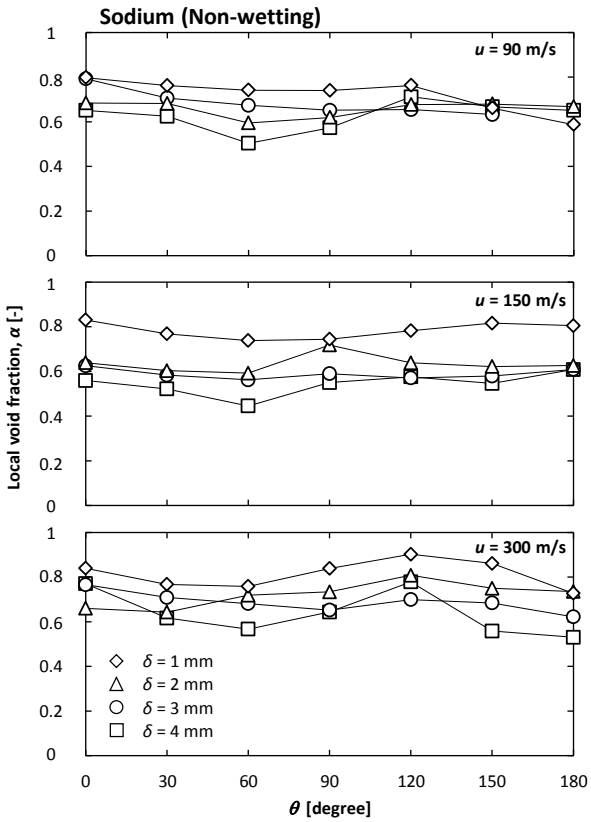


Figure 6 Void fraction distributions around a non-wetting cylinder in liquid sodium

H. Kudoh:

Void Fraction Distributions of Inert Gas Jets across a Single Cylinder with Non-Wetting Surface in Liquid Sodium

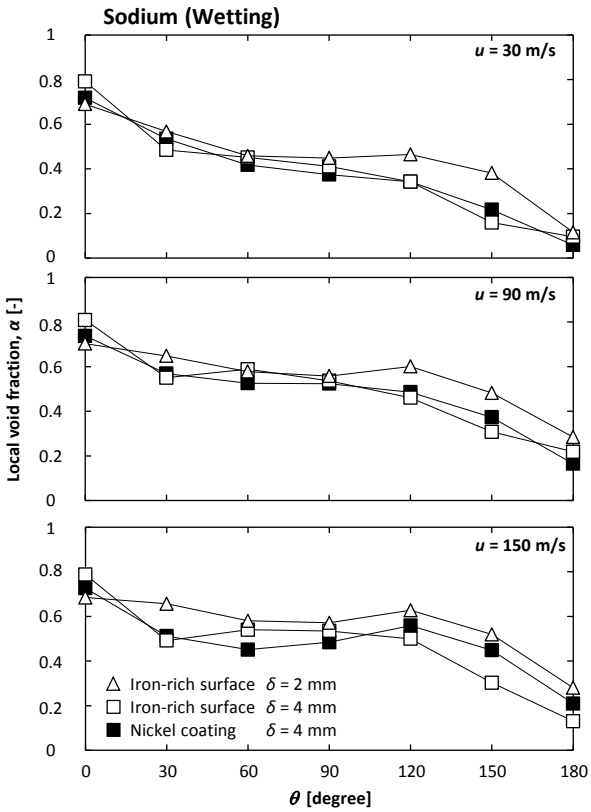


Figure 7 Void fraction distributions around a wetting cylinder in liquid sodium

H. Kudoh:

Void Fraction Distributions of Inert Gas Jets across a Single Cylinder with Non-Wetting Surface in Liquid Sodium

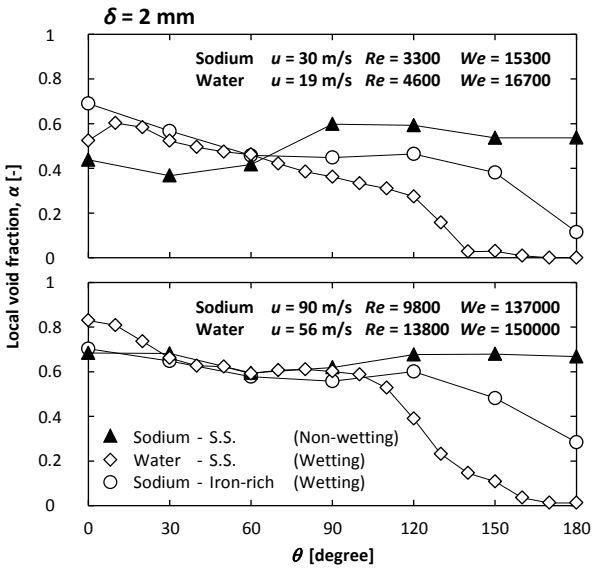


Figure 8 Comparison of void fraction distributions (δ = 2 mm)

H. Kudoh:

Void Fraction Distributions of Inert Gas Jets across a Single Cylinder with Non-Wetting Surface in Liquid Sodium

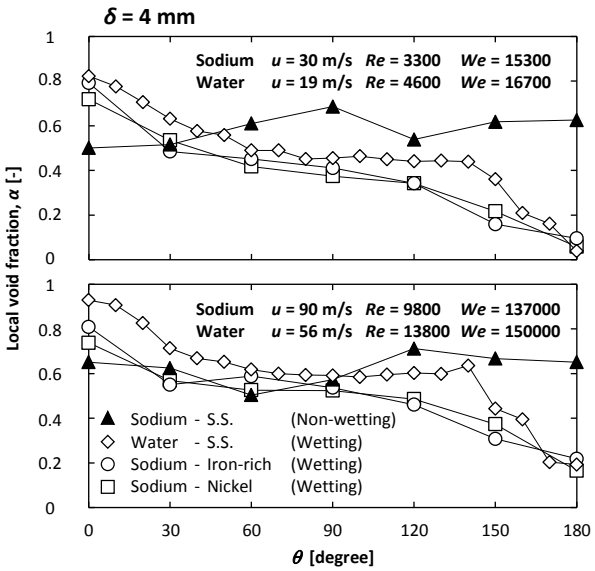


Figure 9 Comparison of void fraction distributions (δ = 4 mm)

H. Kudoh:

Void Fraction Distributions of Inert Gas Jets across a Single Cylinder with Non-Wetting Surface in Liquid Sodium

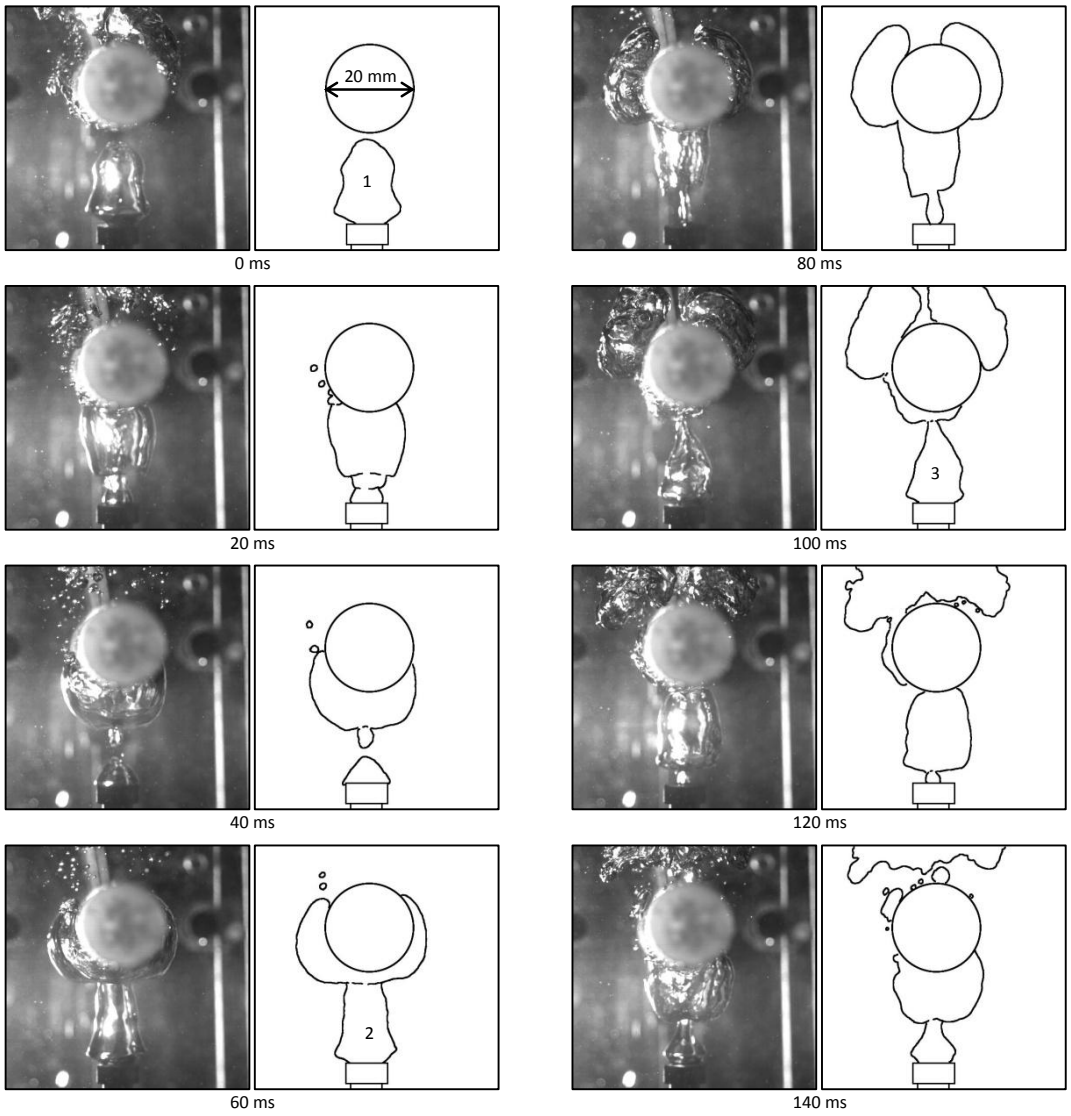


Figure 10 Visualized images of a gas jet around a wetting cylinder (u = 19 m/s)

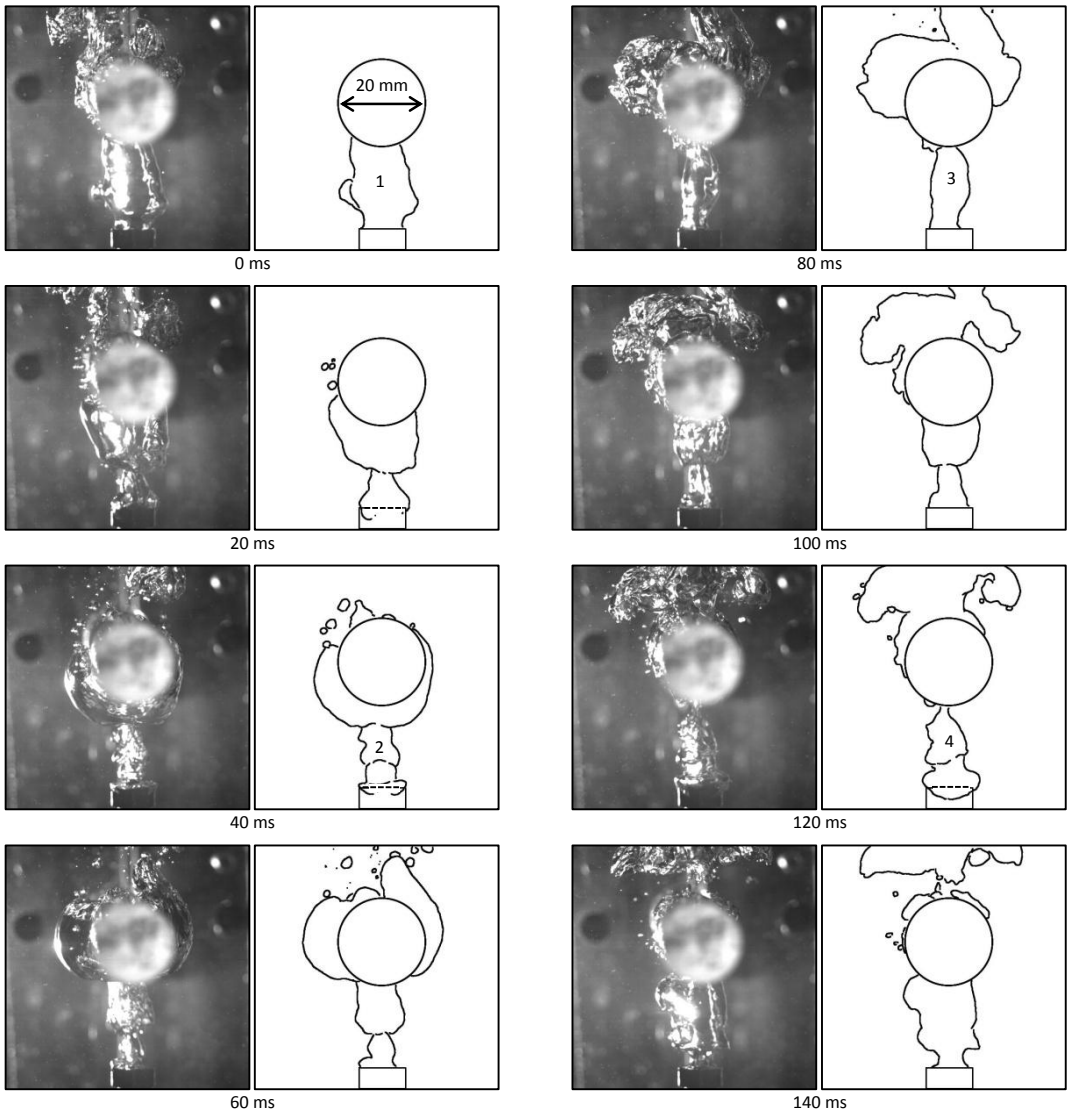


Figure 11 Visualized images of a gas jet around a non-wetting cylinder (u = 19 m/s)